Computer Methods and Programs in Biomedicine 173 (2019) 53–65

Contents lists available at ScienceDirect

Computer Methods and Programs in Biomedicine

journal homepage: www.elsevier.com/locate/cmpb

Automated detection of congestive heart failure from electrocardiogram signal using Stockwell transform and hybrid classification scheme

R.K. Tripathy[a,*], Mario R.A. Paternina[b], Juan G. Arrieta[c], Alejandro Zamora-Méndez[d], Ganesh R. Naik[e]

[a] Department of Electrical and Electronics Engineering, BITS-Pilani, Hyderabad Campus, Hyderabad, 500078, India
[b] Department of Electrical Engineering, National Autonomous University of Mexico, Mexico City, 04510, Mexico
[c] Sanatorio Güemes, Buenos Aires 01188, Argentina
[d] Electrical Engineering Faculty, Universidad Michoacana de San Nicolas de Hidalgo, Morelia, Mich. 58030, Mexico
[e] MARCS Institute, Western Sydney University Kingswood, NSW - 2747, Australia

ARTICLE INFO

Article history:
Received 4 March 2018
Revised 12 February 2019
Accepted 13 March 2019

Keywords:
Congestive heart failure
ECG
Stockwell transform
Time-Frequency entropy
Hybrid classifier
Performance evaluation

ABSTRACT

Background and Objective: The congestive heart failure (CHF) is a life-threatening cardiac disease which arises when the pumping action of the heart is less than that of the normal case. This paper proposes a novel approach to design a classifier-based system for the automated detection of CHF.
Methods: The approach is founded on the use of the Stockwell (*S*)-transform and frequency division to analyze the time-frequency sub-band matrices stemming from electrocardiogram (ECG) signals. Then, the entropy features are evaluated from the sub-band matrices of ECG. A hybrid classification scheme is adopted taking the sparse representation classifier and the average of the distances from the nearest neighbors into account for the detection of CHF. The proposition is validated using ECG signals from CHF subjects and normal sinus rhythm from public databases.
Results: The results reveal that the proposed system is successful for the detection of CHF with an accuracy, a sensitivity and a specificity values of 98.78%, 98.48%, and 99.09%, respectively. A comparison with the existing approaches for the detection of CHF is accomplished.
Conclusions: The time-frequency entropy features of the ECG signal in the frequency range from 11 Hz to 30 Hz have higher performance for the detection of CHF using a hybrid classifier. The approach can be used for the automated detection of CHF in tele-healthcare monitoring systems.

1. Introduction

Congestive heart failure (CHF) is a cardiac ailment, resulting when the heart is unable to deliver a sufficient amount of oxygen and other nutrients to the different parts of the body [1,2]. Its progression causes the heart muscle walls to become weaker so that the lower chambers of the heart are ineffective to pump the blood. The major causes of CHF are the valvular disease, alcoholism, hypertension, myocardial infarction, and diabetes [3]. The cardiac output is reduced due to the cardiac ailments such as left ventricular hypertrophy and left ventricular systolic dysfunction [4–6]. Therefore, the heart fails to deliver the required amount of blood to the whole body conveying to CHF. In developing countries, more than five million elderly people are suffering from CHF pathology, and this number may increase due to the consequence of the diseases like diabetes, myocardial ischemia, and hypertrophic cardiomyopathy [7,8]. The electrocardiogram (ECG) and cardiac echocardiography are normally used for the diagnosis of CHF. The ECG is a simple and low-cost non-invasive diagnostic modality for measuring the electrical activity of the cardiac chambers [9,10]. The CHF is diagnosed through the pathological symptoms such as the changes in the RR-interval and other morphological features in ECG [9,11]. The medical practitioners visually assess the pathological changes in the ECG data during arrhythmia by monitoring inside the coronary care unit. This process is cumbersome due to the low sensitivity in detecting the heart ailments [10]. The early detection of CHF is an important and challenging issue in clinical practice to minimize its progression. Thus, an automated system based on the analysis of the ECG signal is required for the detection of CHF.

* Corresponding author at. Department of Electrical and Electronics Engineering, BITS-Pilani, Hyderabad Campus, Hyderabad, 500078, India.
E-mail address: tripathyrk@hyderabad.bits-pilani.ac.in (R.K. Tripathy).

https://doi.org/10.1016/j.cmpb.2019.03.008
0169-2607/

In recent years, different approaches have been proposed for the automated detection of CHF using the ECG signal [12]. These approaches are focused on the extraction of various diagnostic features from ECG and RR-time series, and the classification of CHF and normal sinus rhythm (NSR) [13–15]. Thuraisingham [16] has used features from the second order difference plot of RR-time series and K-nearest neighbor (K-NN) classifier to discriminate between NSR and CHF. Kuntamalla et al. have calculated sequential trend analysis and multiscale entropy features from the RR-time series [17,18] and have reported a higher classification result for NSR and CHF classes. Hossel et al. [19] have used power spectral densities from the sub-band signals of the RR-time series as features for the detection of CHF. In [20], the same authors have proposed wavelet filters and soft decision algorithm for the detection of CHF from the RR-time series. Yu et al. [21] have used heart rate variability (HRV) features with mutual information based on feature ranking and support vector machine (SVM) for the detection of CHF. Isler and Kuntalap [22] have considered HRV features, wavelet entropy features, and K-nearest neighbor (K-NN) to classify CHF and NSR. Pechia et al. [23] have introduced the time-domain and frequency-domain HRV features, and a simple threshold-based classifier to detect CHF. Despite the aforementioned approaches have demonstrated a suitable performance for the detection of CHF, they have only used the features from the RR-time series. In addition to the HRV features, other morphological features of ECG have presented different values in CHF pathology [9]. Thus, a robust approach founded on the analysis of the ECG signal can be useful for the automated detection of CHF. Note that, a few methods have been reported for the detection of CHF using the features from ECG signal. Among them, Masetic and Subasi have introduced the auto-regressive (AR) model based on features from the ECG signal and the random forest classifier for the detection of CHF [24]. Sudarshan et al. [5] have used the dual-tree complex wavelet transform based on features from ECG and various classification techniques such as K-NN and decision tree for the classification of CHF and NSR.

The abovementioned corroborates that the search of novel feature extraction methods and classification techniques is an important step for the automated detection of heart ailments from the ECG signal [25]. Recently, different time-frequency analysis methods have been widely used for the analysis of RR-time series and ECG signals [26,27], enabling to quantify the diagnostic features from physiological signals in the time-frequency domain; such methods are based on the short-time Fourier transform (STFT) and wavelet transform (WT). The demerits of the STFT are the poor temporal resolution for the high-frequency components and improper frequency resolution for the low-frequency events of a multicomponent signal [28]. Whereas the wavelet transform does not provide phase information since it just produces time-scale plots which require the postprocessing such as synchrosqueezing for obtaining the time-frequency representation of a signal [29]. The Stockwell (S)-transform is the generalization of STFT for a Gaussian window, which has been used to denoise the ECG signal and to detect the QRS-complex [30,31]. This time-frequency analysis method uses variable window length to control the frequency parameter, and the phase information can be obtained with the help of the Fourier kernel. When a CHF occurs, there are variations arising in amplitudes and the durations of the clinical patterns such as QRS-complex, P-wave and T-wave of the ECG signal [32,33]. In fact, it can be expected that the extraction of features using the S-Transform based time-frequency decomposition will be helpful to efficiently assess various pathological changes in ECG signal during CHF. This paper advocates a novel approach to develop an automated system for the detection of CHF. The time-frequency entropy features are evaluated using the Stockwell (S)-transform of the ECG signal and the Shannon Entropy. A hybrid classification scheme-based system that is composed of the class-specific sparse representation based classifier (SRC) and the average distances has been developed for the pattern classification problem in [34]. The kernel SRC has been used for the detection of diabetes using the HRV features in [35]. Unlike the classifiers such as SVM, neural network and deep neural networks, the SRC has fewer parameters (sparsity and iterations), requiring less training instances for the evaluation of the optimal training parameters [34]. It can be expected that the combination between the time-frequency entropy features from ECG and the hybrid classification scheme will be effective to classify CHF and NSR episodes. The rest of this paper is organized as follows. The proposed system is described in Section 2. The results and the discussion of the results are shown in Section 3, and the conclusions of this paper are written in Section 4.

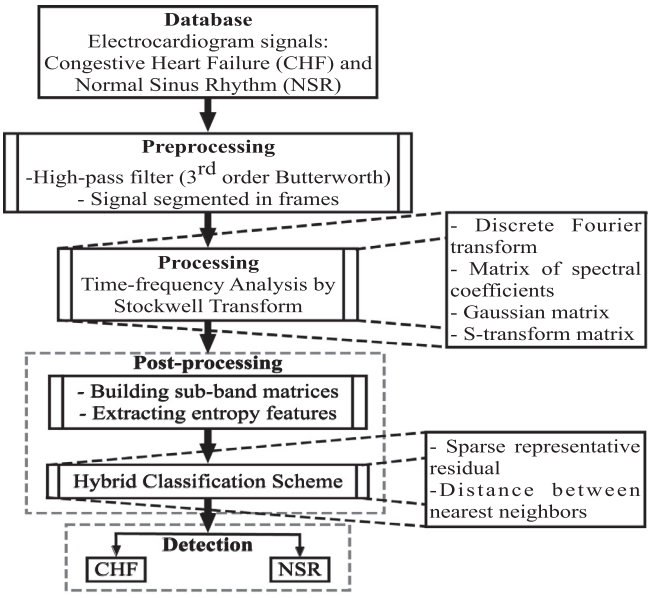

Fig. 1. Flow-chart of the proposed approach for CHF detection.

2. Method

The flow-chart of the proposed approach for the detection of CHF is shown in Fig. 1. The approach consists of four major stages such as the preprocessing of ECG signals, the decomposition of ECG signal into time-frequency sub-band matrices based on the S-transform and frequency division, the evaluation of the time-frequency entropy features, and the hybrid classification scheme. The following sections briefly describe each stage of the proposed approach.

2.1. ECG Database

In this work, we have used CHF and NSR ECG signals from the Beth Israel Deaconess Medical Center (BIDMC) CHF database and the Massachusetts Institute of Technology-Beth Israel Hospital (MIT-BIH) arrhythmia database, respectively [36,37]. The BIDMC CHF database consists of two-lead ECG signals from 15 subjects. These signals are annotated as CHF with class III-IV as per the New York Heart Association (NYHA). Each signal in this database lasts 66.6 min with a sampling frequency of 250 Hz. Likewise, the MIT-BIH arrhythmia database contains 17 NSR ECG signals, each signal lasts for 30 min and has a sample rate of 360 Hz. To be consistent with the BIDMC CHF database, each NSR ECG signal from the MIT-BIH database has been re-sampled to 250 HZ for the analysis. In this study, the first channel ECG signal has been taken into account

from both databases. The correlation coefficient measure is considered to evaluate the similarity between the ECG channels from the databases of two groups. The correlation for the first channel ECG signals from one group database to other group database is obtained as 0.79. Similarly, the correlation between the first channel in one group of the database and the second channel in another group database is found as 0.12. Due to the higher correlation, the first channel ECG signals from both these databases are considered for the analysis. Moreover, the RR-time series data from the CHF RR-interval, MIT-BIH NSR, and NSR RR-interval databases have been used in this work [38]. The MIT-BIH NSR database consists of 18 two-lead ECG signals, and each ECG signal has a sampling frequency of 128 Hz. Similarly, the NSR RR-interval database consists of a RR-time series data from 54 subjects. Likewise, the CHF RR-interval database contains a RR-time series data from 29 subjects. In this study, the RR-time series is extracted from each ECG signal for all the databases using Pan-Tomkin's QRS detection algorithm [39]. The RR-time series data from 44 CHF subjects and 48 NSR subjects are used in this work.

2.2. Preprocessing

In this study, a Butterworth high-pass filter with a cut-off frequency value of 0.5 Hz has been used to remove the baseline wandering noise from the ECG signals of both CHF and NSR classes from the BIDMC CHF and MIT-BIH arrhythmia databases, respectively [40]. Then, the filtered ECG is divided into instances or frames, and each frame has a 4 sec duration (1000 samples). In literature, the frame based approach has been used for the detection of CHF (frame size of 18s, 20s, 2s) and other pathologies from ECG signal in [5,40–43]. Motivated from these studies, we have considered 4s ECG segments or frames for the analysis. In this work, 7667 and 15000 frames are evaluated for NSR (17 subjects) and CHF classes (15 subjects), respectively. We have considered 7667 HC and 7680 CHF 4s ECG frames for the analysis and classification. Each ECG frame is subjected to time-frequency analysis using S-transform.

2.3. Time-Frequency based decomposition of ECG

In this work, the time-frequency analysis of an ECG signal is performed using S-Transform. For an ECG signal $x(n)$ with $n = 1, 2, \ldots, N$, the time-frequency matrix is calculated using four steps [44,45]. Where N is the number of samples in each ECG frame. In the first step, the Discrete Fourier Transform (DFT) of the ECG signal is evaluated, and it is given by [46]

$$y(k) = \sum_{n=1}^{N} x(n) e^{\frac{-j2\pi nk}{N}} \tag{1}$$

Second, the matrix $\mathbf{F} \in R^{K \times N}$ is formulated using the DFT coefficients of an ECG signal, and it is given as

$$\mathbf{F} = \begin{bmatrix} y(2) & y(3) & . & . & . & y(N) & y(1) \\ y(3) & y(4) & . & . & . & y(1) & y(2) \\ . & . & . & . & . & . & . \\ . & . & . & . & . & . & . \\ . & . & . & . & . & . & . \\ y(K) & y(K+1) & . & . & . & y(K-2) & y(K-1) \\ y(K+1) & y(K+2) & . & . & . & y(K-1) & y(K) \end{bmatrix} \tag{2}$$

where $K = \frac{N}{2}$ corresponding the maximum frequency of the signal, and $k = 1, 2, \ldots, K$. Third, the Gaussian matrix in the frequency domain is computed as [28]

$$\mathbf{W} = \begin{bmatrix} w(1,1) & w(1,2) & . & . & . & w(1,N) \\ w(2,1) & w(2,2) & . & . & . & w(2,N) \\ . & . & . & . & . & . \\ . & . & . & . & . & . \\ . & . & . & . & . & . \\ w(K-1,1) & w(K-1,2) & . & . & . & w(K-1,N) \\ w(K,1) & w(K,2) & . & . & . & w(K,N) \end{bmatrix} \tag{3}$$

where each element of the Gaussian matrix is evaluated as $w(k,n) = e^{-\frac{2\pi^2 n^2}{k^2}}$ with $k = 1, 2, \ldots K$ and $n = 1, 2, \ldots, N$, respectively. The Gaussian window matrix is then multiplied with the $\mathbf{F}$ matrix to obtain the windowed frequency domain representation of the ECG signal, and it is given as $\mathbf{H} = \mathbf{FW}$ [47]. The matrix $\mathbf{H}$ can be written as

$$\mathbf{H}_{K,N} = \begin{bmatrix} h(1,1) & h(1,2) & . & . & . & h(1,N) \\ h(2,1) & h(2,2) & . & . & . & h(2,N) \\ . & . & . & . & . & . \\ . & . & . & . & . & . \\ . & . & . & . & . & . \\ h(K-1,1) & h(K-1,2) & . & . & . & h(K-1,N) \\ h(K,1) & h(K,2) & . & . & . & h(K,N) \end{bmatrix} \tag{4}$$

In the last step, the S-transform matrix or the time-frequency matrix from the ECG signal is calculated using the inverse DFT [46]. The S-transform matrix is denoted as Y and $k = 1, 2, \ldots, \frac{N}{2}$. This S-transform matrix quantifies the instantaneous phasor for each frequency component of the ECG signal [46]. In this study, we have applied fast discrete S-transform for the analysis of ECG signal [47]. The window width is determined using frequency-based optimization which is based on the maximization of the concentration measure (CM) [48]. Here, the contour plots represent the S-transform matrix of the ECG signal. The time-frequency contour plots for CHF and NSR ECG signals are depicted in Fig. 2. It has been observed that the morphologies of the contour plots are different for CHF and NSR subjects. For NSR, the peaks are more stretched in the frequency axis as compared to the CHF subject. Higher intensity or amplitude values (as marked in yellow color) of the ECG components from 8 Hz to 30 Hz are observed in the contour plot for the NSR case. From the contour plot of the CHF case, it is also noted that the high intensity values have been shifted to the low-frequency regions. Here, the time-frequency S-transform matrix of the ECG signal (0.5 Hz to 50 Hz) is decomposed into five sub-band matrices or scales based on the frequency division and each sub-band matrix has a size of 10×1000. The time-frequency contour plots of the S-transform matrix at five frequency scales (FS) (FS1, FS2, FS3, FS4, and FS5) for the NSR and CHF cases are depicted in Fig. 3(a)-(j), respectively. Significant differences in the characteristics of the contour plots are observed for the CHF and NSR cases at each sub-band matrix. The 5th, 10th, 15th and 20th frequency components for NSR and CHF classes are shown in Fig. 4(a) and (b), respectively. It is evident that the amplitude values are different for the NSR and CHF cases at these frequency components. The frequency components are more regular in the NSR case as compared to CHF. Therefore, it can be expected that the time-frequency entropy features extracted from these frequency components of each sub-band matrix will be useful for the automated detection of CHF.

2.4. Time-frequency entropy features

In this study, we have extracted the time-frequency entropy features based on the Shannon entropy of each frequency compo-

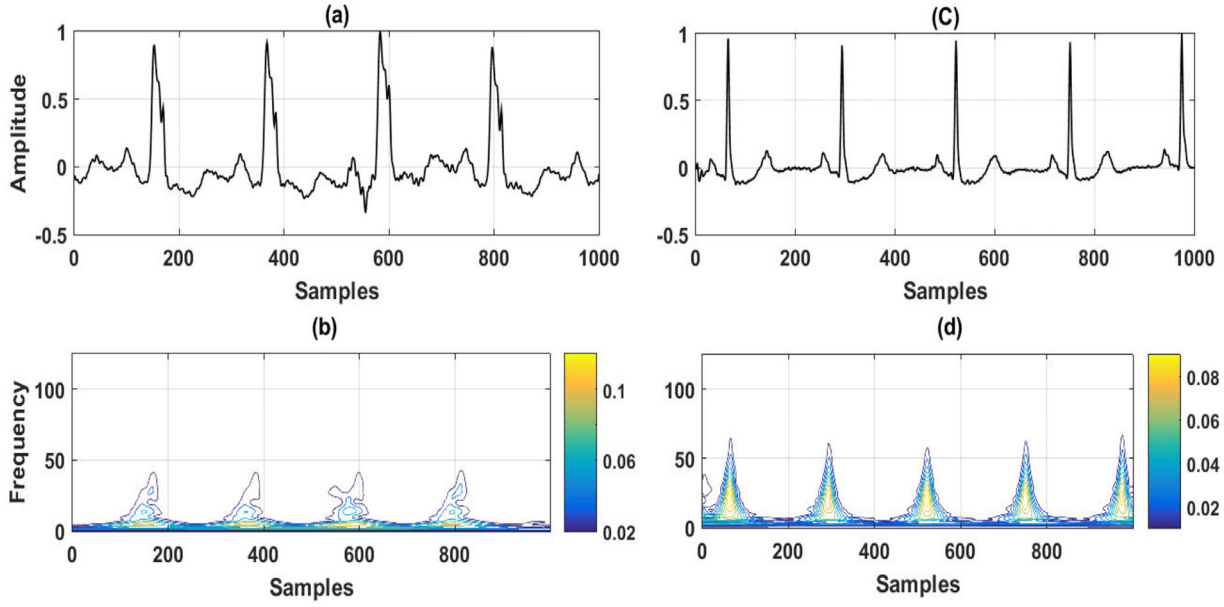

Fig. 2. (a) ECG signal for CHF subject. (b) Time-Frequency plot for CHF ECG signal. (c) NSR ECG Signal. (d) Time-frequency plot for NSR ECG signal.

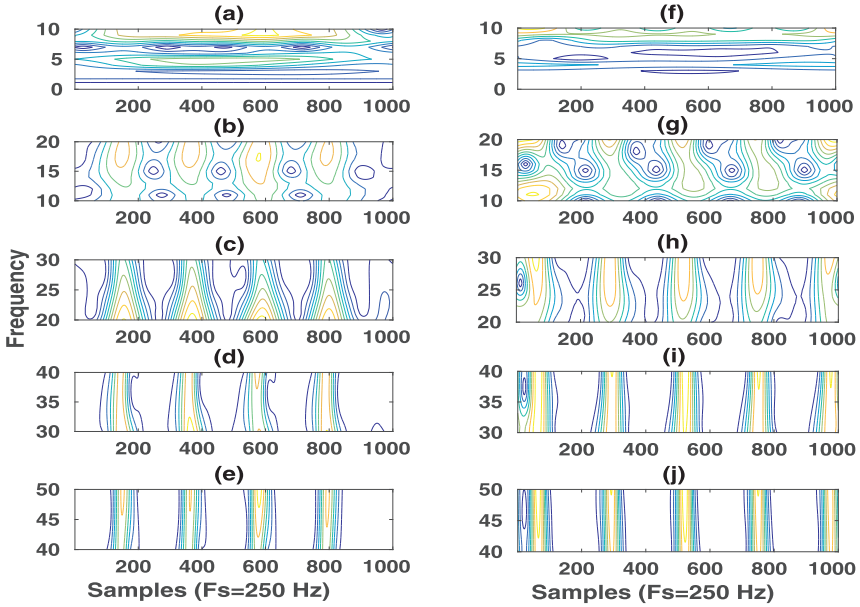

Fig. 3. (a)-(e) Time-frequency contour plots for CHF ECG signal at FS1, FS2, FS3, FS4, and FS5, respectively. (f)-(j) Time-frequency contour plots for NSR ECG signal at FS1, FS2, FS3, FS4, and FS5, respectively.

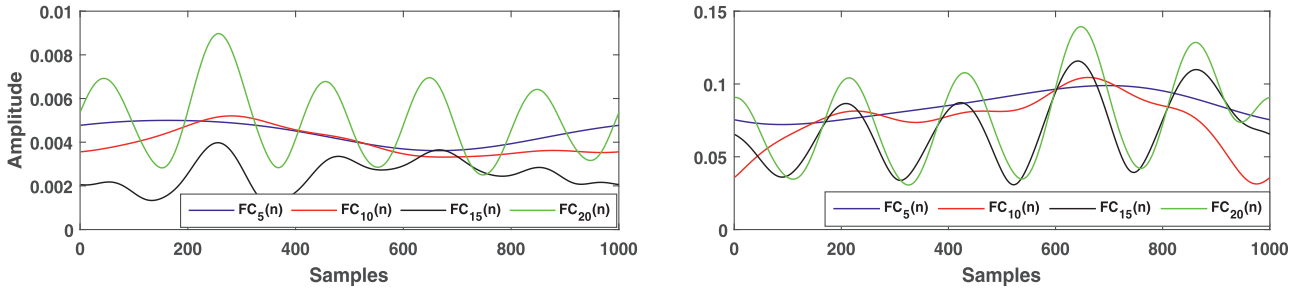

Fig. 4. (a) The 5th, 10th, 15th and 20th frequency components (FCs) for NSR. (b) The 5th, 10th, 15th and 20th frequency components (FCs) for CHF.

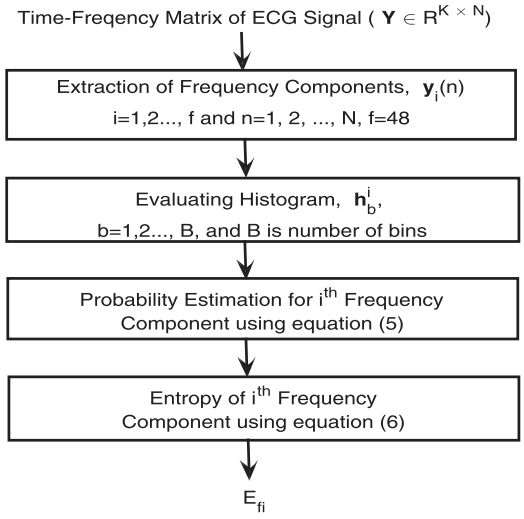

Fig. 5. Flow chart for the evaluation of entropy features from the time-frequency matrix of ECG.

nent from the sub-band matrices of the ECG signal for NSR and CHF classes. The flow-chart for the evaluation of entropy features from the time-frequency matrix is depicted in Fig. 5. For evaluating the entropy measure, only one parameter is required. This parameter is the number of bins in the histogram of each frequency component. The explanations of the step-step procedure for the evaluation of the entropy measure are given as follows. Each sub-band matrix contains 10 frequency components. The histogram of each frequency component is evaluated by considering a number of bins as $B = 10$. The histogram plots for the NSR and CHF cases at 10th and 15th frequency components are shown in Fig. 6(a) and (b), respectively. The values or frequency at each bin is different for the NSR and CHF cases at each frequency component. The probability value for each bin of the ith frequency component is given by

$$P_b^i = \frac{h_b^i}{\sum_{b=1}^{B} h_b^i} \tag{5}$$

where h_b^i is the total number of amplitude values at bth bin for ith frequency component. The time-frequency entropy feature vector is defined as the entropy value of the ith frequency component, and it is given by [49]

$$E_{fi} = -\sum_{b=1}^{B} [P_b^i] log_2 [P_b^i] \tag{6}$$

Here, the entropy features are computed from the first 48 frequency components. A 48 dimensional feature vector is evaluated from each ECG frame or instance. This 48 dimensional feature vector is given as the input to the hybrid classifier. The following subsection describes the hybrid classification scheme for the classification of CHF and NSR.

2.5. Hybrid classification scheme

In this work, we have proposed a hybrid classifier for the classification of CHF and NSR from the time-frequency entropy features of ECG signal. The hybrid classifier is formulated taking into account the class specific sparse representation residual and the average of the distances among the nearest neighbors for each class [34]. The feature matrix $\mathbf{Z} \in R^{m \times d}$ which consists of 'm' instances or examples, and d features are given as, $\mathbf{Z} = [\mathbf{z}_1, \mathbf{z}_2, \ldots, \mathbf{z}_m]$ with each $\mathbf{z}_i \in R^d$ and $i = 1, 2, \ldots, m$. The class label vector corresponds to the feature matrix is denoted as $\mathbf{t}$. This vector consists of the class label of ith example as $\mathbf{t} = [t_1, t_2, \ldots, t_m]$. Here, the feature matrix is divided into training and test data matrices using both hold-out and K-fold cross-validation approaches. The training and test feature data matrices are denoted as $\mathbf{Z1} \in R^{m1_c \times q} = [\mathbf{z1}_1, \mathbf{z1}_2, \ldots, \mathbf{z1}_{m1_c}]$ and $\mathbf{Z2} \in R^{m2_c \times q} = [\mathbf{z2}_1, \mathbf{z2}_2, \ldots, \mathbf{z2}_{m2_c}]$, respectively and $\mathbf{z1}_i \in R^d$ and $\mathbf{z2}_i \in R^d$. Where c corresponds to class indices with $c \in (N, C)$ and, N and C are the class label notations for NSR and CHF classes, respectively. In class specific sparse representation based classifier, the test instance $\mathbf{z}_v$ is represented as the linear combination of the training instances of cth class which is given by $\mathbf{z}_v = \alpha_{1c}\mathbf{z1}_{1c} + \alpha_{1c}\mathbf{z1}_{1c} + \ldots + \alpha_{m1_c c}\mathbf{z1}_{m1_c c}$. This can also be written as [34]

$$\mathbf{z}_v = [\alpha_{1v}, \alpha_{2c}, \ldots, \alpha_{m1_c c}][\mathbf{z1}_{1c}, \mathbf{z1}_{2c}, \ldots, \mathbf{z1}_{m1_c c}] \tag{7}$$

For all classes, the $\mathbf{z}_v$ can be represented as $\mathbf{z}_v = \alpha\mathbf{Z1}$. Where α corresponds to the weight vector, and the combination between the weight vectors of the NSR and CHF classes is defined as $\alpha = [\alpha_N, \alpha_C]$. For the NSR class, the α_C is a zero vector. Similarly, the α_N is also a zero vector for the CHF class. The optimization problem for evaluating the weight vector α is given by [50]

$$\tilde{\alpha} = \arg\min_{\alpha} \quad \|\alpha\|_0$$
$$\text{such that} \quad \mathbf{z}_v = \alpha\mathbf{Z1}$$

The above optimization problem is NP-hard, thereby it is approximately solved using the famous orthogonal matching pursuit (OMP) based greedy algorithm [51]. In OMP, the objective is to select the training instances which produces the highest inner product with the residual of a test instance at each epoch or iteration [51]. The OMP algorithm will be terminated when the number of the selected training instances is higher than the sparsity level defined by the user. The residual for the cth class is calculated using the weight vector $\tilde{\alpha}$ as

$$r_c = \|\mathbf{z}_v - \tilde{\alpha}_c\mathbf{Z1}_c\|_2 \tag{8}$$

For a single test instance, the residual r_c has two values, that is, r_N for NSR and r_C for CHF. Similarly, for the cth class, the Euclidean distances (ED) between the test instance and the 'Q' number of nearest training instances are evaluated, so that the qth ED is given by

$$Ed_c^q = \left\|\mathbf{z}_v - \mathbf{z1}_c^q\right\|_2 \tag{9}$$

where $q = 1, 2, \ldots, Q$, and Q is the number of nearest neighbors for the cth class. The average of the distances of the cth class is given by $d_c^{\mu} = \frac{1}{Q}\sum_{q=1}^{Q} Ed_c^q$. Similarly, the median of the distances for the jth class is also computed by $d_c^{md} = Median_{q=1,2,\ldots,Q}(Ed_c^q)$. For the cth class, the total distance (TD) for a test instance $\mathbf{z}_v$ is defined as the linear combination between the residual, and the mean or median distance. The TD using mean metrics is defined by $TD_c^{\mu} = r_c + d_c^{\mu}$. Similarly, the $TD_c^{md} = r_c + d_c^{md}$ is termed as the TD using median metric. The class label for $\mathbf{z}_v$ is evaluated based on the expression as,

$$t_v = arg\ min_{c \in (N,C)}(TD_c^{\mu}) \tag{10}$$

In this study, the performance of the test instances is accessed using class specific SRC (CSSRC), hybrid classifiers with mean metric (HCMM), and hybrid classifier with median metric (HCMDM). The main dataset contains 15,347 ECG instances (7667 NSR ECG instances and 7680 CHF ECG instances) and 48 features. This main dataset or feature matrix is first divided into both training dataset and test dataset based on either hold-out or 10-fold cross-validation. The hold-out cross-validation contains 80% of the dataset for training the CSSRC and hybrid classifiers, whereas the remaining 20% are considered for evaluation or testing. Similarly, during 10-fold cross-validation, 90% of the dataset is used for the training at each fold, whereas the remaining 10% of the dataset

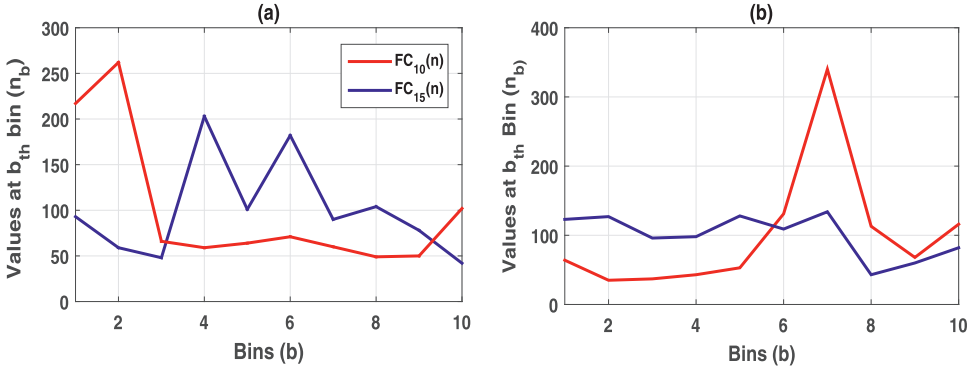

Fig. 6. (a) Histogram plots of 10th and 15th frequency components (FCs) for NSR. (b) Histogram plots of 10th and 15th frequency components (FCs) for CHF.

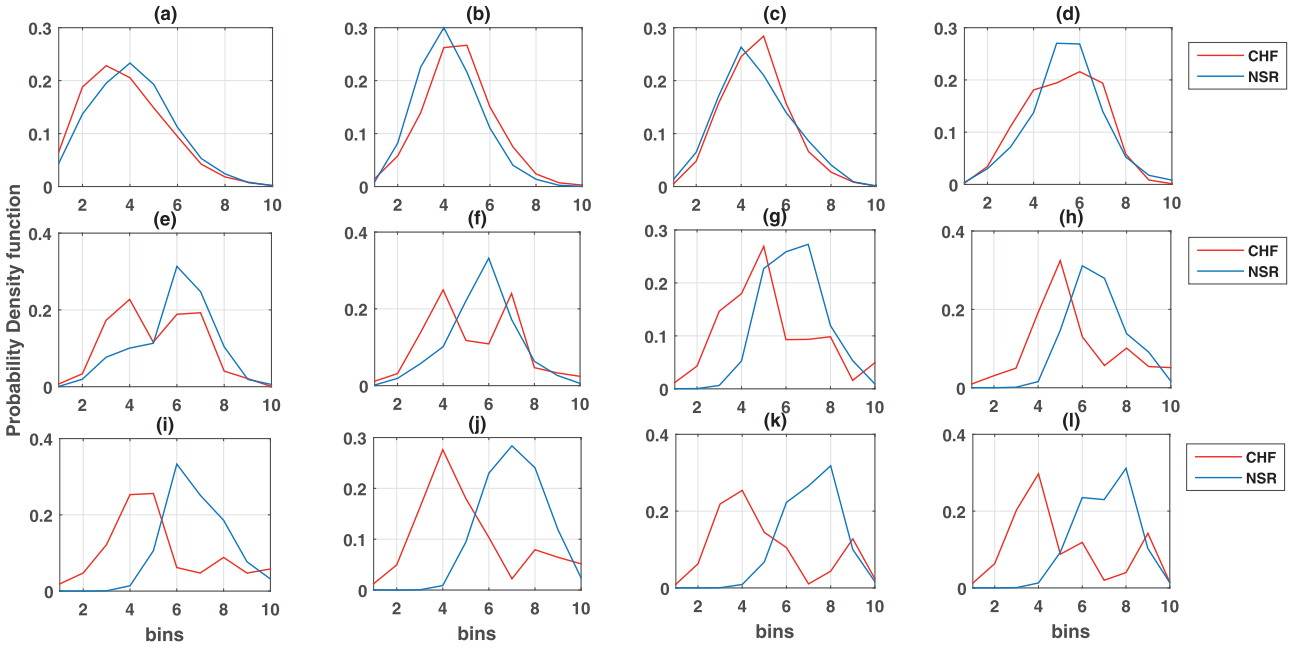

Fig. 7. Plots of the probability density function (PDF) associated with the entropy features for the NSR and CHF classes, corresponding to the: (a) 2nd frequency component; (b) 4th frequency component; (c) 7th frequency component; (d) 10th frequency component; (e) 12th frequency component; (f) 15st frequency component; (g) 21th frequency component; (h) 27th frequency component; (i) 31st frequency component; (j) 35th frequency component; (k) 42nd frequency component; and (l) 47th frequency component.

is evaluated during the testing of the hybrid classifier. The measures such as accuracy, sensitivity, specificity and area under the ROC curve (AROC) are used in order to evaluate the performance of the hybrid classifier [52].

3. Results

The proposed method (as outlined in Fig. 1) is evaluated using both NSR and CHF ECG signals. The time-frequency entropy features are calculated from each ECG instance for both CHF and NSR classes. The statistical analysis of the time-frequency entropy features for NSR and CHF classes and the performance of the hybrid classifier are described in this section. The plots of the probability density function (PDF) associated with the selected time-frequency entropy features for NSR and CHF classes are displayed in Fig. 7(a)-(l). It is notable that the probability values and the bin locations for the peaks in the PDF plots are different for the NSR and CHF classes. The entropy features from 31st, 35th, 42nd, and 47th frequency components illustrate higher discrimination in the PDF plots as compared to the entropy features of lower frequency components. In CHF pathology case, the major spectral energy of the ECG signal is distributed from 0.5 Hz up to 40 Hz, and the spectral amplitude values are less after 30 Hz frequency component [12]. Due to this fact, the higher differences in the peak values for high-frequency entropy features are observed in PDF plots for the CHF and NSR classes. The mean and the standard deviation values of the entropy features for the selected frequency components from the time-frequency sub-band matrices of ECG instances are depicted in Table 1 for the NSR and CHF classes. It is evident that the entropy features have higher mean values for CHF class in the low frequency components (first, third, fourth, fifth and eighth frequency components (E_{f1}, E_{f3}, E_{f4}, E_{f5} and E_{f8})) of the ECG signal. From the contour plot in Fig. 2, we have noted that for CHF case there is the shift in the high-intensity values to the low-frequency region. The ECG patterns during CHF are abnormal caused by the consequence of pathologies such as left ventricular hypertrophy and left ventricular dysfunction, respectively [53]. The low-frequency components of the QRS-complex have higher amplitude values in the spectrum of ECG signal due to the variation of the QRS-interval. This may be the reason that yields higher mean values in the entropy features for the CHF class. Apart from the low-frequency components, the entropy features from other frequency components have the lower mean values for the CHF class. The NSR ECG signals have a higher beat to beat variability as

Table 1
Statistical analysis of time-frequency entropy features.

Features	NSR ($\mu \pm \sigma$)	CHF ($\mu \pm \sigma$)	p-value
E_{f3}	2.38 ± 0.98	2.59 ± 1.08	< 0.001
E_{f4}	2.52 ± 0.92	2.77 ± 1.04	< 0.001
E_{f5}	2.56 ± 0.87	2.66 ± 1.02	< 0.001
E_{f7}	2.90 ± 0.89	2.88 ± 1.00	0.301
E_{f8}	2.98 ± 0.82	3.08 ± 1.11	< 0.001
E_{f11}	3.56 ± 0.88	3.25 ± 1.10	< 0.001
E_{f14}	3.90 ± 0.77	3.72 ± 1.27	< 0.001
E_{f17}	4.10 ± 0.85	3.86 ± 1.13	< 0.001
E_{f19}	4.34 ± 0.72	4.07 ± 1.12	< 0.001
E_{f21}	4.54 ± 0.65	4.16 ± 1.09	< 0.001
E_{f24}	4.63 ± 0.60	4.25 ± 1.00	< 0.001
E_{f28}	4.60 ± 0.66	4.26 ± 1.11	< 0.001
E_{f30}	4.55 ± 0.65	4.25 ± 1.11	< 0.001
E_{f32}	4.50 ± 0.62	4.23 ± 1.16	< 0.001
E_{f36}	4.37 ± 0.58	4.14 ± 1.18	< 0.001
E_{f38}	4.31 ± 0.56	4.11 ± 1.17	< 0.001
E_{f41}	4.24 ± 0.53	4.06 ± 1.12	< 0.001
E_{f43}	4.20 ± 0.53	4.02 ± 1.08	< 0.001
E_{f45}	4.14 ± 0.54	3.95 ± 1.01	< 0.001
E_{f48}	4.04 ± 0.54	3.91 ± 0.97	< 0.001

compared to the pathological case. Since the reduction in left ventricular ejection fraction in CHF, the QRS complex amplitude in ECG is reduced, and also the CHF case ECG signal is less chaotic as compared to NSR caused by less beat-to-beat variations [53]. Henceforth, the entropy features in this range have lower mean values for CHF class. The student *t*-test has been used for the evaluation of the statistical significance of the proposed time-frequency entropy features [54]. From the *t*-test results, it is inferred that 47 time-frequency entropy features have the p-values less than 0.001 and only the Entropy feature from the seventh frequency component (E_{f7}) of the ECG signal has a p-value of 0.301. Therefore, 47 entropy features of the ECG signal are found to be statistically significant. In this study, we have used all 48 entropy features for the classification of the CHF and NSR classes.

The performance of the time-frequency entropy features from the ECG signal is accessed using the CSSRC, HCMM and HCMDM classifiers. Here, the 48 dimensional feature vector is divided into three sub-vectors. The entropy features from the first ten frequency components are termed as low-frequency entropy features. Similarly, the entropy features from the 11th to 30th frequency components are considered as mid-band frequency (MBF) entropy features. Likewise, the entropy features from the 31st to 48th frequency components are used as high-frequency (HF) entropy features. The Fisher score (F-score) is used to evaluate the rank of each feature in 48 dimensional feature vector [52]. The F-score value of each time-frequency entropy feature is illustrated in Fig. 8. It is evident that maximum features in the MBF range have higher F-score values as compared to the scores for LF and HF entropy features. The performance of LF entropy feature vector, MBF entropy feature vector, HF entropy feature vector, and 48 dimensional time-frequency entropy feature vector is accessed using the CSSRC, HCMM, and HCMDM classifiers. The accuracy, the sensitivity, the specificity and the AROC values for these classifiers using hold-out cross-validation are depicted in Table 2. It is evident that the accuracy, sensitivity and specificity values of HCMM classifier with LF entropy features are higher than HCMDM and CSSRC classifiers. However, the AROC values are similar for HCMM and HCMDM classifiers. When MBF features are used, the HCMDM classifier has higher accuracy, sensitivity and specificity values compared to other classifiers. Similarly, the performance of HCMM is higher using HF entropy features. The diagnostic information of the T-wave and the low-frequency component of P-wave of ECG are captured in the frequency range from 0.5 Hz to 10 Hz [55]. Moreover, the frequency range from 30 Hz to 48 Hz in ECG captures the high-frequency component of QRS-complex [55]. It has also been noted that the HF entropy features have higher performance with all classifiers as compared to the LF features. When all features are used, the HCMM classifier has the accuracy, sensitivity, specificity and AROC values of 98.78%, 98.48%, 99.09% and 0.98, respectively. These values are highest as compared to the performance of other classifiers. Notice that the performance of HCMM is higher than CSSRC. The CSSRC uses only residual of the sparse representation of test instances for classification. However, HCMM combines the residual with the distances between the K-nearest neighbors for each class to achieve the highest values of accuracy, sensitivity, and specificity. The ROC curves for CSSRC, HCMM and HCMDM classifiers using all entropy features are displayed in Fig. 9. It is observed that the HCMM classifier has an AROC value of 0.986, which is higher than the AROC values for both HCMDM and CSSRC classifiers.

The performance of HCMM with the LF, MBF, HF, and all entropy features are evaluated using a 10-fold cross-validation based selection of ECG instances, as depicts in Table 3. From the results, it is evident that the accuracy, sensitivity, and specificity values are higher than 97% in each fold using all entropy features. At each fold, the performance of HCMM is higher using MBF entropy features as compared to LF and HF entropy features. The performance of HCMM is also evaluated using the time-frequency entropy features of ECG signals from both the MIT-BIH NSR database and CHF database, respectively. The accuracy, sensitivity and specificity values of HCMM for 10-fold cross-validation approach are illustrated in Table 4. The average for the accuracy, sensitivity, and specificity values is high at each fold using all entropy features. We have used two feature selection techniques such as correlation based feature selection (CFS) and principle component analysis (PCA) based on feature projection and selection for choosing a few features out of the 48 dimensional feature vector and the feature selection steps have the advantage to reduce the computational complexity of the classifier [56,57]. A total of 29 features is selected out of 48 features using CFS, which are used as the input to all classifiers. Moreover, in the PCA domain, we have selected 20 features based on the higher Eigenvalues. The performance of classifiers is evaluated by considering feature selection techniques for hold-out, and 10-fold cross-validation schemes, as exhibits in Tables 2 and 3, respectively. It is evident that there are very small variations in the accuracy, sensitivity, and specificity values for all classifier after selecting a few features. Similarly, for the 10-fold cross-validation case, when the selected features are considered the accuracy values for HCMM classifier along all folds are similar as compared to the performance for all features. The NSR and CHF ECG signals have frequency ranges as [0.1–40 Hz] and [0.1–100 Hz], respectively [36–38]. For the NSR case, we have divided the LF, MBF and HF ranges as 0.1–10 Hz, 11–50 Hz, and 51–100 Hz. Similarly, for the CHF case, the frequency ranges for LF, MBF, and HF bands are 0.1–10 Hz, 11–30 Hz, and 30–40 Hz, respectively. We have evaluated one entropy feature from each time-frequency matrix. A three dimensional feature vector is created for the NSR and CHF instances using the entropy features from the LF, HF and MBF time-frequency matrices. The performance of this feature vector is evaluated using the classifiers for hold-out and 10-fold cross-validation cases, as displays in Tables 2 and 3, respectively. It has been noted that by controlling the frequency ranges of ECG signals for the NSR and CHF cases; the accuracy, sensitivity, and specificity are reduced as compared to the performance of the LF, HF, MBF, and selected time-frequency entropy features. Moreover, we have also evaluated time-frequency features from RR-time series data for the detection of CHF. These features are the mean values of the first ten frequency components from the S-transform matrix of the RR-time series. The performance of these time-frequency features of the RR-time series is evaluated using the hybrid classifier

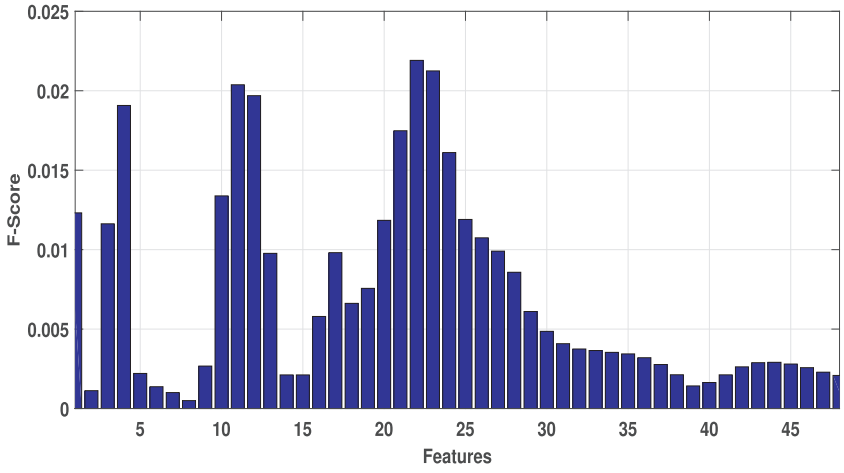

Fig. 8. Ranking of each time-frequency entropy feature using F-score.

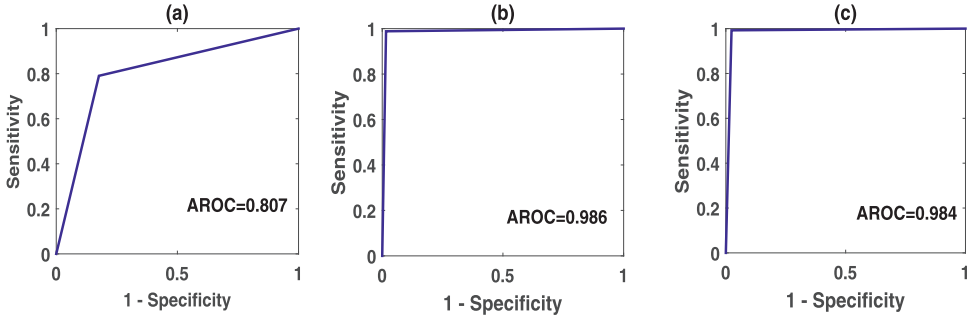

Fig. 9. ROC curve for classifiers using all features: (a) CSSRC; (b) HCMM; and (c) HCMDM.

Table 2
Performance of CSSRC, HCMM and HCMDM using selected and all entropy features. (Acc-Accuracy, Sen-Sensitivity, and Spe-Specificity).

Feature Selection	Classifiers	Acc(%)	Sen(%)	Spe(%)	AROC(%)
Features with Different Frequency Range (DFR)	CSSRC	47.59 ± 1.63	46.34 ± 1.33	49.24 ± 2.38	0.47 ± 1.23
	HCMM	54.73 ± 1.81	54.44 ± 3.41	55.02 ± 3.11	0.54 ± 3.01
	HCMDM	53.93 ± 1.46	53.74 ± 2.48	54.11 ± 2.89	0.53 ± 1.32
LF Entropy Features	CSSRC	52.19 ± 0.74	53.03 ± 1.14	51.36 ± 0.75	0.52 ± 0.01
	HCMM	84.01 ± 0.69	84.31 ± 0.88	83.71 ± 1.26	0.83 ± 0.01
	HCMDM	83.56 ± 0.37	83.59 ± 0.83	83.52 ± 0.87	0.83 ± 0.01
MBF Entropy Features	CSSRC	59.70 ± 0.21	57.06 ± 3.11	62.34 ± 2.85	0.59 ± 0.01
	HCMM	97.32 ± 0.28	96.53 ± 0.93	98.11 ± 0.46	0.97 ± 0.00
	HCMDM	97.44 ± 0.43	97.76 ± 0.62	98.12 ± 0.31	0.97 ± 0.01
HF Entropy Features	CSSRC	53.73 ± 1.23	38.21 ± 2.15	69.26 ± 3.31	0.53 ± 0.01
	HCMM	89.23 ± 0.48	87.93 ± 0.48	90.53 ± 0.98	0.88 ± 0.01
	HCMDM	88.71 ± 0.21	86.47 ± 0.61	90.94 ± 0.80	0.88 ± 0.01
All Entropy Features	CSSRC	81.82 ± 0.32	84.89 ± 0.96	78.74 ± 0.67	0.81 ± 0.01
	HCMM	98.78 ± 0.15	98.48 ± 0.35	99.09 ± 0.12	0.98 ± 0.00
	HCMDM	98.64 ± 0.31	98.34 ± 0.19	98.93 ± 0.45	0.98 ± 0.01
PCA based Feature Projection and Selection	CSSRC	72.50 ± 0.82	77.48 ± 2.30	67.53 ± 1.24	0.71 ± 0.01
	HCMM	98.53 ± 0.25	98.28 ± 0.36	98.78 ± 0.32	0.98 ± 0.00
	HCMDM	98.33 ± 0.33	97.96 ± 0.35	98.70 ± 0.32	0.98 ± 0.00
Correlation based Feature Selection (CFS)	CSSRC	77.10 ± 0.79	83.95 ± 1.14	70.26 ± 1.08	0.77 ± 0.01
	HCMM	97.73 ± 0.18	97.41 ± 0.30	98.05 ± 0.25	0.97 ± 0.00
	HCMDM	97.58 ± 0.21	97.20 ± 0.35	97.96 ± 0.69	0.97 ± 0.00

with 10-fold cross-validation, as illustrates in Table 5. It is observed that the average accuracy, average sensitivity, and average specificity values are 70.92%, 68.27% and 73.58%, respectively and these values are less than the performance of the time-frequency features of ECG signal. In CHF, there are the variations in the ECG clinical patterns such as the shortening of the duration of QRS-complex and the attenuation of the amplitude values of both P-wave and QRS-complex [58–61]. The proposed time-frequency features fail to capture the pathological changes due to the minute morphological and temporal variations in the RR-time series. In the clinical standard, the analysis of a short duration (5 min) RR-time series is performed for the physiological interpretation [62]. In this study, we have evaluated time-frequency features from 5 min duration RR-time series segments for the detection of CHF. Given this

Table 3
Performance of HCMM using LF, MBF, HF and all entropy features, and 10-fold cross-validation. (Acc-Accuracy, Sen-Sensitivity, and Spe-Specificity).

Features	Measures	Fold1	Fold2	Fold3	Fold4	Fold5	Fold6	Fold7	Fold8	Fold9	Fold10	Average
DFR	**Acc(%)**	51.83	55.58	55.41	58.91	54.58	56.50	63.33	55.08	57.08	58.41	56.67 ± 3.08
	Sen(%)	54.50	56.33	56.00	70.00	59.50	53.50	61.83	56.66	59.33	57.33	58.50 ± 4.73
	Spe(%)	49.16	54.83	54.83	47.83	49.66	59.50	64.83	53.50	54.83	59.50	54.85 ± 5.30
LF	**Acc(%)**	84.25	82.83	82.33	83.66	83.58	82.91	82.33	84.75	85.16	83.16	83.50 ± 0.97
	Sen(%)	84.50	82.50	84.50	85.33	85.16	81.83	83.83	84.00	85.50	84.16	84.13 ± 1.18
	Spe(%)	84.00	83.16	80.16	82.00	82.00	84.00	80.83	85.50	84.83	82.16	82.86 ± 1.72
MBF	**Acc(%)**	96.66	97.91	97.25	97.41	97.91	97.50	98.25	96.75	96.66	97.41	97.37 ± 0.55
	Sen(%)	95.66	97.83	96.33	96.50	97.16	96.66	97.83	95.66	95.66	95.66	96.50 ± 0.87
	Spe(%)	97.66	98.00	98.16	98.33	98.66	98.33	98.66	97.83	97.66	99.16	98.25 ± 0.48
HPF	**Acc(%)**	88.33	88.16	89.00	87.83	88.41	90.58	88.41	87.75	89.66	89.33	88.75 ± 0.89
	Sen(%)	86.00	85.50	89.33	85.66	85.83	89.33	87.33	85.50	87.00	88.66	87.01 ± 1.57
	Spe(%)	90.66	90.83	88.66	90.00	91.00	91.83	89.50	90.00	92.33	90.00	90.48 ± 1.08
All	**Acc(%)**	98.50	98.50	98.58	98.66	99.08	98.58	99.25	98.50	98.75	98.41	98.68 ± 0.27
	Sen(%)	97.83	98.00	98.50	97.83	98.83	98.66	98.83	98.00	98.00	98.83	98.33 ± 0.43
	Spe(%)	99.16	99.00	98.66	99.50	99.33	98.50	99.66	99.00	99.50	98.00	99.03 ± 0.52
PCA	**Acc(%)**	98.33	98.33	98.33	99.25	98.25	98.33	98.25	98.16	99.08	98.00	98.43 ± 0.40
	Sen(%)	98.33	97.33	98.33	99.50	97.16	97.33	98.00	97.33	99.00	98.00	98.03 ± 0.78
	Spe(%)	98.33	99.33	98.33	99.00	99.33	99.33	98.50	99.00	99.16	98.00	98.83 ± 0.49
CFS	**Acc(%)**	97.41	97.58	97.16	96.58	98.16	97.41	98.33	97.83	98.66	98.08	97.72 ± 0.61
	Sen(%)	97.00	97.16	96.66	96.50	98.00	97.00	98.50	97.66	98.66	97.00	97.41 ± 0.75
	Spe(%)	97.83	98.00	97.66	96.66	98.33	97.83	98.16	98.00	98.66	99.16	98.03 ± 0.65

Table 4
Performance of hybrid classifier using ECG signals from the MIT BIH NSR and CHF databases. (Acc-Accuracy, Sen-Sensitivity, and Spe-Specificity.).

Measures	Fold1	Fold2	Fold3	Fold4	Fold5	Fold6	Fold7	Fold8	Fold9	Fold10	Average
Acc (%)	98.33	98.25	98.41	98.83	98.83	98.41	98.83	99.08	98.41	98.75	98.61 ± 0.28
Sen (%)	98.16	97.33	97.83	98.66	98.33	97.83	98.66	98.66	98.50	98.50	98.25 ± 0.45
Spe (%)	98.50	99.16	99.00	99.00	99.33	99.00	99.00	99.50	98.33	99.00	98.98 ± 0.34

Table 5
Performance of hybrid classifier using time-frequency features from the RR-time series. (Acc-Accuracy, Sen-Sensitivity, and Spe-Specificity.).

Measures	Fold1	Fold2	Fold3	Fold4	Fold5	Fold6	Fold7	Fold8	Fold9	Fold10	Average
Acc (%)	69.46	71.00	70.75	71.40	71.31	71.15	71.96	69.68	70.37	72.15	70.92 ± 0.88
Sen (%)	67.00	67.87	68.87	69.25	68.00	67.06	69.00	67.37	67.50	70.81	68.27 ± 1.20
Spe (%)	71.93	74.12	72.62	73.56	74.62	75.25	74.93	72.00	73.25	73.50	73.58 ± 1.16

short-interval-based analysis of the RR-time series, the meaningful clinical information may be lost for the detection of CHF. Thereby, this fact does that the accuracy, sensitivity and specificity values of HCMM classifier are less using time-frequency features from RR-time series. Altan et al. [12] have reported the accuracy, sensitivity and specificity values of 97.83%, 100%, and 93.79% for the detection of CHF using 3 h segment of the RR-time series. In the future, the time-frequency analysis of long duration RR-time series data can be performed for the detection of CHF.

In this study, the number of frequency components for the evaluation of time-frequency features is selected using the grid-search technique. The average accuracy values of HCMM classifier are evaluated by varying the number of frequency components for the time-frequency entropy features and these values are exhibited in Table 6, where it is noted that the average accuracy is maximum when the number of frequency components is equal to 48. The average accuracy value reduces by increasing the number of frequency components. In the ECG signal, the frequency ranges between 0.5 to 50 Hz captures major spectral energy [55] and due to the presence of noise after the 50th frequency component, the average accuracy value is reduced. In literature, the ECG frame specific approaches have been used for the detection of CHF [5,24,41]. Furthermore, to verify the effectiveness of the proposed method,

Table 6
Variation of Average accuracy with the number of frequency components for time-frequency entropy features.

Number of Frequency Components	Average Accuracy (%)
40	98.54
43	98.54
45	98.66
48	99.16
52	99.00
55	98.91
60	98.91

the patient specific cross-validation approach is accomplished for evaluating the performance of HCMM classifier. In patient specific cross-validation approach, the ECG instances from a particular patient are used for the testing of the classifier, whereas the remaining ECG instances from the other patients and NSR based ECG instances are used for the training [63]. The individual classification accuracy values for the ECG instances for different CHF patients are shown in Table 7. Notice that the performance of HCMM is higher for CHF 01, CHF 03, CHF 05, CHF 06, CHF 09, CHF 11, CHF 13 and CHF 15 subjects based on the patient specific cross-validation approach. For other subjects, the performance of HCMM may degrade

Table 7
Accuracy value of HCMM classifier using CHF patient specific cross-validation approach.

Record Number	Accuracy (%)
CHF01	100
CHF02	42.14
CHF03	81.84
CHF04	20.51
CHF05	100
CHF06	62.30
CHF07	17.58
CHF08	13.67
CHF09	100
CHF10	41.41
CHF11	99.02
CHF12	18.36
CHF13	85.55
CHF15	84.38

due to minute pathological variations into the ECG signal. We have also compared the performance of the hybrid classifier using the time-frequency entropy features from ECG frames with different durations, as shows in Table 8. It is observed that the 2s duration ECG segment time-frequency entropy features with HCMM classifier have higher performance for the detection of CHF. Therefore, the 2s ECG segment is considered as the optimal duration in the proposed approach for the detection of CHF. For this work, we have evaluated 45334, 30212, 22667, 18137, 15090, 12934, and 11325 number of 2s, 3s, 4s, 5s, 6s, 7s and 8s ECG segments from all the ECG recordings. Due to more number of ECG instances are evaluated in the testing phase, the hybrid classifier has a higher performance using 2 sec ECG instances as compared to other duration ECG segments. We have also computed the number of P, Q, R, S, and T wave points for different duration (1s to 8s) ECG segments, and these values are shown in Table 8. Note that the 8s segment captures 10, 9, 9, 9 and 9 no. of P, Q, R, S, and T points of the ECG signal. Though, the 8s ECG segment correctly captures diagnostic information of the ECG signal; in this study, we have extracted only 11325 no. of 8s ECG instances which is less than the number of 2s ECG instances from the ECG recordings of the database. Given the less number of ECG instances that are evaluated using a hybrid classifier, the accuracy value of this classifier is reduced to 96.36%.

4. Discussion

The objective of this study is the detection of CHF based on the time-frequency analysis of the ECG signal. The time-frequency features from LF, MBF and HF components of ECG signal are extracted using S-transform and entropy measure. The hybrid classification technique is used for assessing the performance of the proposed time-frequency entropy features of the ECG signal. To verify the effectiveness of the proposed approach, we have compared our results with existing CHF (type III -IV) detection methods. The comparison result has been exhibited in Table 9. The state-of-art methods for the detection of CHF (type I-II-III) have used features from RR-time series. The proposed approach only considers type III-IV CHF instances. The existing methods require an extra pre-processing stage such as the detection of R-peaks for evaluation of HRV and other features, which may increase the computing time. Along with the diagnostic features of RR-time series, there are the variations in the other morphological features of ECG signal in CHF pathology. Kamath [41] has evaluated detrend fluctuation analysis (DFA) features from 20 sec ECG segments for the detection of CHF. In another study, the same author has extracted various entropy features from 18 sec ECG segment for the detection of CHF. Thus, the performance of these two methods are comparable with the proposed approach, they have used longer duration ECG signal for the analysis. In [24], authors have used AR model coefficients as features from 2.77 sec ECG data for the detection of CHF. Despite this method achieved a very high accuracy value for the detection of CHF pathology; it requires the selection of model order as prior to the analysis of the ECG signal. The method reported in [5] used the statistical features from the complex wavelet coefficients of 2 sec ECG data for the detection of CHF. The accuracy, sensitivity, and specificity reported in this study was 99.86%, 99.78%, and 99.94%, respectively. The selection of appropriate basis functions and the decomposition levels are required for the evaluation of real and complex wavelet coefficients. The proposed approach evaluates the features directly from the ECG signal based on the time-frequency analysis, and it does not require the detection of R-peaks and the selection of decomposition level. The performance of the proposed work is also compared with the wavelet-based time-scale approach for the detection of CHF. Daqrouq and Dobaie have used the wavelet energy features of ECG and confirmation functions based classification approach for the detection of CHF [65]. They have reported an accuracy value of 92.60% for the classification of NSR and CHF. We have also evaluated the performance of the wavelet entropy features using a hybrid classifier, and the accuracy value is obtained as 62.97%. The summary of the proposed work is written as follows.

- The time-frequency entropy features computed using the S-transform of ECG signal accurately quantify the diagnostic information for the automated prediction of the CHF pathology.
- The performance of HCMM classifier using time-frequency features ECG signal is higher than the features from short duration RR-time series.
- The hybrid classifier, based on the combination of the sparse representation residual and nearest neighbors, is used for the detection of CHF using time-frequency features from the ECG signal and RR-time series.
- Most of the entropy features in the MBF range have higher F-score values compared to other entropy features.
- The performance of the hybrid classifier using time-frequency entropy features in the frequency range from 10 Hz to 30 Hz is higher than the features from other frequency components.

Table 8
Performance of hybrid classifier with time-frequency entropy features from ECG segments with different durations.

ECG duration	Accuracy (%)	Sensitivity (%)	Specificity (%)	P-points	Q-points	R-points	S-points	T-points
1s	99.27 ± 0.15	98.90 ± 0.31	99.65 ± 0.30	2	1	1	1	1
2s	99.37 ± 0.25	99.13 ± 0.41	99.61 ± 0.28	3	3	2	2	2
3s	99.12 ± 0.20	98.98 ± 0.37	99.26 ± 0.30	4	4	4	3	3
4s	98.68 ± 0.27	98.33 ± 0.43	99.03 ± 0.52	5	5	5	5	4
5s	98.16 ± 0.38	98.10 ± 0.65	98.23 ± 0.55	6	6	6	6	5
6s	97.38 ± 0.34	97.00 ± 0.57	97.76 ± 0.54	7	7	7	7	7
7s	97.39 ± 0.53	97.42 ± 0.61	97.35 ± 0.70	9	8	8	8	8
8s	96.36 ± 0.97	96.36 ± 1.45	96.36 ± 0.89	10	9	9	9	9

Table 9
Comparison with existing approaches. (Acc-Accuracy, Sen-Sensitivity, Spe-Specificity, and NR-Not reported).

Authors	Features Used	Classifier Used	Acc (%)	Sen (%)	Spe (%)	Instances Used	CHF Type
Kuntamalla and reddy [17]	Sequential trend analysis of RR-time series	K-nearest neighbor	96.68	100	94.44	33 (33 subjects)	I-II-III
Hossen and Al-Ghunaimi [19]	Sub-band DFT spectral patterns of RR-time series	Threshold based Classification	87.14	76.50	90.50	70 (70 subjects)	I-II-III
Asyali [15]	HRV Features	Bayesian Classifier	NR	81.80	98.10	74 (74 subjects)	I-II-III
Pechia et al. [23]	HRV Features	Classification and regression trees	96.40	89.70	100	83 (83 subjects)	I-II-III
Hossen and Al-Ghunaimi [20]	Wavelet based features from RR-time series	Threshold based Classification	96.3	93.3	100	97 (97 subjects)	I-II-III
Yu and Lee [21]	HRV Features and conditional mutual information	Quadratic classifier	97.59	96.55	98.14	83 (83 subjects)	I-II-III
Isler and Kuntalp [22]	HRV and wavelet entropy features of RR-time series, and genetic algorithm	K-nearest neighbor	93.98	100	91.53	83 (83 subjects)	I-II-III
Altan et al. [12]	Statistical features from IMFs from RR-time series	Multilayer Perceptron Network	97.83	100	93.79	83 (83 subjects)	I-II-III
Kamath (a) [41]	DFA Features from 20s ECG	Threshold Classifier	98.20	98.40	98.00	7020 (15 subjects)	III-IV
Kamath (b) [42]	Entropy Features from 18s ECG	Threshold Classifier	99.90	100	99.00	6435 (33 subjects)	III-IV
Liao et al. [64]	ECG samples as Features	SVM Classifier	97.27	NA	NA	33 subjects	III-IV
Masetic and Subasi [24]	AR model parameters of ECG	RF Classifier	100	NA	NA	31 subjects	III-IV
Sudarshan et al. [5]	DTCWT based ECG Features	Decision tree Classifier	99.86	99.78	99.94	142051 (73 subjects)	III-IV
Proposed work	Time-frequency entropy features from 4s ECG	HCMM	98.78	98.48	99.09	15347 (32 subjects)	III-IV

- The method has higher accuracy value than the performance of wavelet-based features for the classification of CHF and NSR ECG signals.

The advantages of the proposed work are written as follows. In ECG signal, the frequency ranges for the clinical components such as T-wave, P-wave, and QRS-complex have been reported as [0.5–10 hz], [5–30 Hz] and [8–50 Hz], respectively [55]. In some recent studies, it has been found that the frequency range above 24 Hz is most informative since it captures the information about the high-frequency components of QRS-complex of ECG signal [55,66]. From this work, it has been noted that the frequency range from 11 to 30 Hz of the ECG signal shows higher variations during CHF. From literature, it has been reported that the electrocardiographic changes such as ST-segment depression, T-wave inversion, change in the QRS-complex duration, decrease in the amplitude of QRS-complex, reduction in the P-wave amplitude and variation in the QT-interval are observed in CHF pathology. The MBF range (11 Hz-30 Hz) captures the major spectral energy of P-wave and QRS-complex of ECG signal [55]. It has also been reported that the attenuation of QRS-complex voltage and the prolongation of QRS-complex duration in ECG are the symptoms of heart failure [32,33]. These pathological changes in ECG signal for CHF patients alter the values of MBF range entropy features. Due to these reasons, the performance of HCMM classifiers is high using MBF time-frequency entropy features as compared to LF and HF entropy features. The HCMM classifier combines the decisions of the class specific sparse representation residuals and the average of the distances from the nearest neighbours, whereas the HCMDM classifier considers the median of the distances of the nearest neighbours. The average measure considers all the distances from the nearest instances for evaluating the overall distance; meanwhile the median is evaluated using the middle value of the distances from the nearest neighbours. Hence, the HCMM classifier has higher performance as compared to CSSRC and HCMDM classifiers. In this study, the analysis of the time-frequency phase components of the ECG signal has not been used for the detection of CHF. Various features can be extracted from the phase of the S-transform time-frequency matrix of the ECG signal.

In this work, the performance of the proposed approach has been evaluated separately using both the RR-time series and ECG signal. The intermediate step in the Pan Tompkin's algorithm is the use of a band-pass filter with cutoff frequencies as 5 Hz and 11 Hz, respectively for the QRS-complex detection and the evaluation of R-peaks [39]. However, in the present work, we have directly applied S-transform and frequency division over the ECG signal for the evaluation of time-frequency matrices. The frequency components are not affected since as we have not used any low-pass filter over the ECG signal to extract the time-frequency entropy features. Zidelmal et al. [31] have used the S-transform and Shannon energy for the detection of R-peaks from the ECG signal. They have extracted the frequency band, [5–22.5 Hz] from the spectrogram of the ECG signal, and have evaluated local Shannon energy in the selected frequency band to create an envelope. The R-peaks are detected from the Shannon energy envelope using thresholding. They have reported the sensitivity value of 99.84% which is higher than the Pan-Thompkin's algorithm for the QRS-complex detection. The S-transform method has higher performance for the detect R-peaks in noisy and pathological ECG signals [31]. To verify the effectiveness of the proposed approach, we have extracted the RR-time series from the ECG signals using both Pan-Thompkin's and S-transform based R-peak detection algorithm. The characteristics of RR-time series signals are similar using both algorithms. The Pan-Thompkin's algorithm is simple as compared to the S-transform for the R-peak detection from the ECG signal. Therefore, we have considered Pan-Thompkin's algorithm for the extraction of

RR-time series from the ECG signal. In this study, we have found that the time-frequency features which are evaluated based on the S-transform analysis of the RR-time series have less accuracy, sensitivity and specificity values for the detection of CHF. Hence, more robust features based on the use of other time-frequency analysis approaches can be extracted from the RR-time series. The non-linear measures such as entropy features, detrended fluctuation analysis, recurrent quantification analysis (RQA), correlation dimension (CD) and higher order spectra (HOS) [67] can be computed from the time-frequency components of RR-time series for the detection of CHF. Here, we have only used the accuracy, sensitivity and specificity measures for evaluating the performance of the classifier. Henceforth, other measures such as the Matthew's correlation coefficient, F-measure can also be used [52,68]. It is an interesting problem in clinical practice for the prediction of CHF in patients with myocardial infarction, cardiomyopathy, and valvular diseases. In the future, the new signal processing approaches can be developed to address this problem. Recently, Altan et al. [69] have proposed the second order difference plot (SODP) for the analysis of the ECG signal. They have extracted various features from the SODP of ECG and used these features for human identification. The SODP based features are evaluated directly from the ECG signal and hence, these features capture global information of the ECG signal. However, in the present work, we have extracted entropy features from each frequency component of ECG in the S-transform domain. In the future, the SODP features can be extracted from each frequency component of the time-frequency matrix of ECG for the detection of CHF and other heart diseases. We have also compared the simulation times for the S-transform and wavelet transform-based analysis of ECG signals. The simulation time for the time-scale based-decomposition of the ECG signal using a wavelet-based analysis and synthesis framework is 0.130 sec. Similarly, for evaluating the time-frequency sub-band matrix of ECG signal using S-transform, the simulation time is found to be 0.033 sec which is less than the wavelet-based analysis of ECG. The SVM, the multilayer feed-forward neural network (MFNN) and the relevant vector machine classifiers require very higher computational time for the estimation of training parameters [70]. However, the classification technique used in the proposed approach is simple since it is based on the sparse representation residual and distances from the nearest neighbors.

5. Conclusions

In this paper, a novel approach for the automated detection of CHF based on the time-frequency analysis of the ECG signal has been demonstrated. The time-frequency analysis of ECG was performed using S-transform. From the S-transform coefficients of the ECG signal at different frequency scales, the time-frequency entropy features have been computed. A hybrid classifier based on the combination of the residual of SRC and nearest distance for individual classes was used. The important observation from this work is that the entropy features in the range from 10 Hz to 30 Hz in ECG signal is highly affected during CHF pathology and the performance of the hybrid classifier is highest by using these features. The other entropy measures and various dimension reduction techniques such as independent component analysis (ICA) and linear discriminant analysis (LDA) can be used to quantify the diagnostic information from ECG signal for accurate and reliable detection of CHF pathology. The time-frequency features extracted using the proposed method can be used for the detection of other pathologies from the ECG signal.

Conflict of interest

I declare that there is no conflict of interest for this paper.

6. Acknowledgments including declarations

We would like to thank Editor-in-Chief, Associate editor and anonymous reviewers of this journal for considering our paper for publication. This is purely an academic research work, and the first author (RK Tripathy) has received OPERA award with the grant number as FR/SCM/150618/EEE from BITS Pilani, Hyderabad Campus.

Supplementary material

Supplementary material associated with this article can be found, in the online version, at doi:10.1016/j.cmpb.2019.03.008.

References

[1] C.W. Yancy, M. Jessup, B. Bozkurt, J. Butler, D.E. Casey, M.H. Drazner, G.C. Fonarow, S.A. Geraci, T. Horwich, J.L. Januzzi, et al., 2013 Accf/aha guideline for the management of heart failure: executive summary: a report of the american college of cardiology foundation/american heart association task force on practice guidelines, J. Am. Coll. Cardiol. 62 (16) (2013) 1495–1539.
[2] V.L. Roger, Epidemiology of heart failure, Circ. Res. 113 (6) (2013) 646–659.
[3] E.E. Tripoliti, T.G. Papadopoulos, G.S. Karanasiou, K.K. Naka, D.I. Fotiadis, Heart failure: diagnosis, severity estimation and prediction of adverse events through machine learning techniques, Comput. Struct. Biotechnol. J. 15 (2017) 26–47.
[4] S.A. Hunt, Acc/aha 2005 guideline update for the diagnosis and management of chronic heart failure in the adult: a report of the american college of cardiology/american heart association task force on practice guidelines (writing committee to update the 2001 guidelines for the evaluation and management of heart failure), J. Am. Coll. Cardiol. 46 (6) (2005) e1–e82.
[5] V.K. Sudarshan, U.R. Acharya, S.L. Oh, M. Adam, J.H. Tan, C.K. Chua, K.P. Chua, R. San Tan, Automated diagnosis of congestive heart failure using dual tree complex wavelet transform and statistical features extracted from 2s of ecg signals, Comput. Biol. Med. 83 (2017) 48–58.
[6] S. Gupta, J.D. Berry, C.R. Ayers, S.A. Matulevicius, R.M. Peshock, P.C. Patel, D.W. Markham, M.H. Drazner, Association of health aging and body composition (abc) heart failure score with cardiac structural and functional abnormalities in young individuals, Am. Heart J. 159 (5) (2010) 817–824.
[7] S. Nadar, N. Prasad, R.S. Taylor, G.Y. Lip, Positive pressure ventilation in the management of acute and chronic cardiac failure: a systematic review and meta-analysis, Int. J. Cardiol. 99 (2) (2005) 171–185.
[8] W. Rosamond, K. Flegal, K. Furie, A. Go, K. Greenlund, N. Haase, S.M. Hailpern, M. Ho, V. Howard, B. Kissela, et al., Heart disease and stroke statistics 2008 update: a report from the american heart association statistics committee and stroke statistics subcommittee, Circulation 117 (4) (2008) e25–e146.
[9] J.E. Madias, The resting electrocardiogram in the management of patients with congestive heart failure: established applications and new insights, Pac. Clin. Electrophysiol. 30 (1) (2007) 123–128.
[10] O. Faust, U.R. Acharya, T. Tamura, Formal design methods for reliable computer-aided diagnosis: a review, IEEE Rev. Biomed. Eng. 5 (2012) 15–28.
[11] S.S. Barold, A.L. GOLDBERGER, A specific ecg triad associated with congestive heart failure, Pac. Clin. Electrophysiol. 5 (4) (1982) 593–599.
[12] G. Altan, Y. Kutlu, N. Allahverdi, A new approach to early diagnosis of congestive heart failure disease by using hilbert–huang transform, Comput. Method. Progr. Biomed. 137 (2016) 23–34.
[13] U. Orhan, Real-time chf detection from ecg signals using a novel discretization method, Comput. Biol. Med. 43 (10) (2013) 1556–1562.
[14] Z. Mašetic, A. Subasi, Detection of congestive heart failures using c4. 5 decision tree, Southeast Eur. J. Soft Comput. 2 (2) (2013).
[15] M. Asyali, Discrimination power of long-term heart rate variability measures, in: Engineering in Medicine and Biology Society, 2003. Proceedings of the 25th Annual International Conference of the IEEE, 1, IEEE, 2003, pp. 200–203.
[16] R. Thuraisingham, A classification system to detect congestive heart failure using second-order difference plot of rr intervals, Cardiol. Res. Pract. 2009 (2009).
[17] S. Kuntamalla, L.R.G. Reddy, Detecting congestive heart failure using heart rate sequential trend analysis plot, Int. J. Eng. Sci. Technol. 2 (12) (2010) 7329–7334.
[18] S. Kuntamalla, R.G.R. Lekkala, Reduced data dualscale entropy analysis of hrv signals for improved congestive heart failure detection, Measur. Sci. Rev. 14 (5) (2014) 294–301.
[19] A. Hossen, B. Al-Ghunaimi, Identification of Patients with Congestive Heart Failure by Recognition of Sub-bands Spectral Patterns, 2008.
[20] A. Hossen, B. Al-Ghunaimi, A wavelet-based soft decision technique for screening of patients with congestive heart failure, Biomed. Signal Process. Control 2 (2) (2007) 135–143.
[21] S.-N. Yu, M.-Y. Lee, Conditional mutual information-based feature selection for congestive heart failure recognition using heart rate variability, Comput. Method. Progr. Biomed. 108 (1) (2012) 299–309.
[22] Y. İşler, M. Kuntalp, Combining classical hrv indices with wavelet entropy measures improves to performance in diagnosing congestive heart failure, Comput. Biol. Med. 37 (10) (2007) 1502–1510.

[23] L. Pecchia, P. Melillo, M. Sansone, M. Bracale, Discrimination power of short--term heart rate variability measures for chf assessment, IEEE Trans. Inf. Technol. Biomed. 15 (1) (2011) 40–46.
[24] Z. Masetic, A. Subasi, Congestive heart failure detection using random forest classifier, Comput. Method. Progr. Biomed. 130 (2016) 54–64.
[25] R. Acharya, S.M. Krishnan, J.A. Spaan, J.S. Suri, Advances in cardiac signal processing, Springer, 2007.
[26] Y. Li, W. Pan, K. Li, Q. Jiang, G.-Z. Liu, Sliding trend fuzzy approximate entropy as a novel descriptor of heart rate variability in obstructive sleep apnea, IEEE J. Biomed. Health Inform. (2018).
[27] K. Huang, L. Zhang, Cardiology knowledge free ecg feature extraction using generalized tensor rank one discriminant analysis, EURASIP J. Adv. Signal Process. 2014 (1) (2014) 2.
[28] S.S. Sahu, G. Panda, N.V. George, An improved s-transform for time-frequency analysis, in: Advance Computing Conference, 2009. IACC 2009. IEEE International, IEEE, 2009, pp. 315–319.
[29] A. Ahrabian, D. Looney, L. Stanković, D.P. Mandic, Synchrosqueezing-based time-frequency analysis of multivariate data, Signal Process. 106 (2015) 331–341.
[30] M. Das, S. Ari, Analysis of ecg signal denoising method based on s-transform, Irbm 34 (6) (2013) 362–370.
[31] Z. Zidelmal, A. Amirou, D. Ould-Abdeslam, A. Moukadem, A. Dieterlen, Qrs detection using s-transform and shannon energy, Comput. Method. Progr. Biomed. 116 (1) (2014) 1–9.
[32] J.E. Madias, Mechanism of attenuation of the qrs voltage in heart failure: a hypothesis, Europace 11 (8) (2009) 995–1000.
[33] A. Kashani, S.S. Barold, Significance of qrs complex duration in patients with heart failure, J. Am. Coll. Cardiol. 46 (12) (2005) 2183–2192.
[34] M. Cui, S. Prasad, Class-dependent sparse representation classifier for robust hyperspectral image classification, IEEE Trans. Geosci. Remote Sens. 53 (5) (2015) 2683–2695.
[35] R. Tripathy, M.R.A. PATERNINA, P. Pattanaik, A new method for automated detection of diabetes from heart rate signal, J. Mech. Med. Biol. 17 (07) (2017) 1740001.
[36] D.S. Baim, W.S. Colucci, E.S. Monrad, H.S. Smith, R.F. Wright, A. Lanoue, D.F. Gauthier, B.J. Ransil, W. Grossman, E. Braunwald, Survival of patients with severe congestive heart failure treated with oral milrinone, J. Am. Coll. Cardiol. 7 (3) (1986) 661–670.
[37] G.B. Moody, R.G. Mark, The impact of the mit-bih arrhythmia database, IEEE Eng. Med. Biol. Mag. 20 (3) (2001) 45–50.
[38] A.L. Goldberger, L.A. Amaral, L. Glass, J.M. Hausdorff, P.C. Ivanov, R.G. Mark, J.E. Mietus, G.B. Moody, C.-K. Peng, H.E. Stanley, Physiobank, physiotoolkit, and physionet: components of a new research resource for complex physiologic signals., Circulation 101 (23) (2000) E215–20.
[39] J. Pan, W.J. Tompkins, A real-time qrs detection algorithm, IEEE Trans. Biomed. Eng 32 (3) (1985) 230–236.
[40] L. Sharma, R. Tripathy, S. Dandapat, Multiscale energy and eigenspace approach to detection and localization of myocardial infarction, IEEE Trans. Biomed. Eng. 62 (7) (2015) 1827–1837.
[41] C. Kamath, A new approach to detect congestive heart failure using detrended fluctuation analysis of electrocardiogram signals, J. Eng. Sci. Technol. 10 (2) (2015) 145–159.
[42] C. Kamath, Entropy measures of irregularity and complexity for surface electrocardiogram time series in patients with congestive heart failure, J. Advan. Comput. Res. 6 (4) (2015) 1–11.
[43] A. Hernando, M. Pelaez, M.T.L. Albalate, M. Aiger, D. Izquierdo, A. Sanchez, M.I. Lopez-Jurado, J.I. Moura, J. Fidalgo, J. Lazaro, E. Gil, Autonomic nervous system measurement in hyperbaric environments using ecg and ppg signals, IEEE J. Biomed. Health Inform. PP (99) (2018) 1, doi:10.1109/JBHI.2018.2797982.
[44] R.G. Stockwell, L. Mansinha, R. Lowe, Localization of the complex spectrum: the s transform, IEEE Trans. Signal Process. 44 (4) (1996) 998–1001.
[45] M. Uyar, S. Yildirim, M.T. Gencoglu, An expert system based on s-transform and neural network for automatic classification of power quality disturbances, Expert Syst. Appl. 36 (3) (2009) 5962–5975.
[46] M. Biswal, P.K. Dash, Measurement and classification of simultaneous power signal patterns with an s-transform variant and fuzzy decision tree, IEEE Trans. Ind. Inf. 9 (4) (2013) 1819–1827.
[47] K. Krishnanand, P. Dash, A new real-time fast discrete s-transform for cross-differential protection of shunt-compensated power systems, IEEE Trans. Power Delivery 28 (1) (2013) 402–410.
[48] I. Djurović, E. Sejdić, J. Jiang, Frequency-based window width optimization for s-transform, AEU-Int. J. Electroni. Commun. 62 (4) (2008) 245–250.
[49] T.M. Cover, J.A. Thomas, Elements of Information Theory, Elsevier, United Kingdom, 2012.
[50] R. Rosas-Romero, A. Díaz-Torres, G. Etcheverry, Forecasting of stock return prices with sparse representation of financial time series over redundant dictionaries, Expert Syst. Appl. 57 (2016) 37–48.
[51] J.A. Tropp, A.C. Gilbert, Signal recovery from random measurements via orthogonal matching pursuit, IEEE Trans. Inf. Theory 53 (12) (2007) 4655–4666.
[52] R.O. Duda, P.E. Hart, D.G. Stork, Pattern Classification, John Wiley & Sons, Athens, Greece, 2012.
[53] J.E. Madias, et al., Ecg Changes and Voltage Attenuation in Congestive Heart Failure, Hospital Chronicles 2006, 2006.
[54] T.W. Anderson, The Statistical Analysis of Time Series, Vol. 19, Elsevier, United States (US), 2011.
[55] L.G. Tereshchenko, M.E. Josephson, Frequency content and characteristics of ventricular conduction, J. Electrocardiol. 48 (6) (2015) 933–937.
[56] M.A. Hall, Correlation-based Feature Selection for Machine Learning, 1999.
[57] A. Malhi, R.X. Gao, Pca-based feature selection scheme for machine defect classification, IEEE Trans. Instrum. Meas. 53 (6) (2004) 1517–1525.
[58] J.E. Madias, R. Bazaz, H. Agarwal, M. Win, L. Medepalli, Anasarca-mediated attenuation of the amplitude of electrocardiogram complexes: a description of a heretofore unrecognized phenomenon, J. Am. Coll. Cardiol. 38 (3) (2001) 756–764.
[59] J.E. Madias, Significance of shortening of the mean qrs duration of the standard electrocardiogram in patients developing peripheral edema, Am. J. Cardiol. 89 (12) (2002) 1444–1446.
[60] J.E. Madias, P waves in patients with changing edematous states: implications on interpreting repeat p wave measurements in patients developing anasarca or undergoing hemodialysis, Pac. Clin. Electrophysiol. 27 (6p1) (2004) 749–756.
[61] J.E. Madias, Ecg changes and voltage attenuation in congestive heart failure, Hosp. Chron. 3 (3) (2008) 112–115.
[62] A. Camm, M. Malik, J. Bigger, G. Breithardt, S. Cerutti, R. Cohen, P. Coumel, E. Fallen, H. Kennedy, R. Kleiger, et al., Heart rate variability: standards of measurement, physiological interpretation and clinical use. task force of the european society of cardiology and the north american society of pacing and electrophysiology, Circulation 93 (5) (1996) 1043–1065.
[63] R. Tripathy, U.R. Acharya, Use of features from rr-time series and eeg signals for automated classification of sleep stages in deep neural network framework, Biocyber. Biomed. Eng. (2018).
[64] K.Y.-K. Liao, C.-C. Chiu, S.-J. Yeh, A novel approach for classification of congestive heart failure using relatively short-term ecg waveforms and svm classifier, in: Proceedings of the International MultiConference of Engineers and Computer Scientists, 1, 2015.
[65] K. Daqrouq, A. Dobaie, Wavelet based method for congestive heart failure recognition by three confirmation functions, Comput. Math. Method. Med. 2016 (2016).
[66] B. Gramatikov, V. Iyer, Intra-qrs spectral changes accompany st segment changes during episodes of myocardial ischemia, J. Electrocardiol. 48 (1) (2015) 115–122.
[67] U.R. Acharya, S.V. Sree, P.C.A. Ang, R. Yanti, J.S. Suri, Application of non-linear and wavelet based features for the automated identification of epileptic eeg signals, Int. J. Neural Syst. 22 (02) (2012) 1250002.
[68] S. Boughorbel, F. Jarray, M. El-Anbari, Optimal classifier for imbalanced data using matthews correlation coefficient metric, PLoS ONE 12 (6) (2017) e0177678.
[69] G. ALTAN, Y. KUTLU, M. YENIAD, Ecg based human identification using second order difference plots, Comput. Method. Progr. Biomed. 170 (2019) 81–93.
[70] R.A. Collazo, L.A.M. Pessôa, L. Bahiense, B.d.B. Pereira, A.F.d. Reis, et al., A comparative study between artificial neural network and support vector machine for acute coronary syndrome prognosis, Pesquisa Operacional 36 (2) (2016) 321–343.